Accepted Manuscript

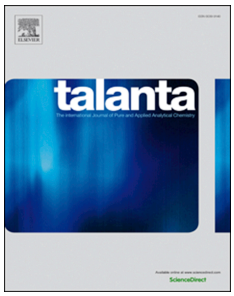

Facile synthesis of IrO_2/rGO nanocomposites with high peroxidase-like activity for sensitive colorimetric detection of low weight biothiols

Xueliang Liu, Xinhuan Wang, Qiusen Han, Cui Qi, Chen Wang, Rong Yang

PII: S0039-9140(19)30564-8

DOI: https://doi.org/10.1016/j.talanta.2019.05.070

Reference: TAL 19955

To appear in: *Talanta*

Received Date: 29 November 2018

Revised Date: 7 May 2019

Accepted Date: 16 May 2019

Please cite this article as: X. Liu, X. Wang, Q. Han, C. Qi, C. Wang, R. Yang, Facile synthesis of IrO_2/rGO nanocomposites with high peroxidase-like activity for sensitive colorimetric detection of low weight biothiols, *Talanta* (2019), doi: https://doi.org/10.1016/j.talanta.2019.05.070.

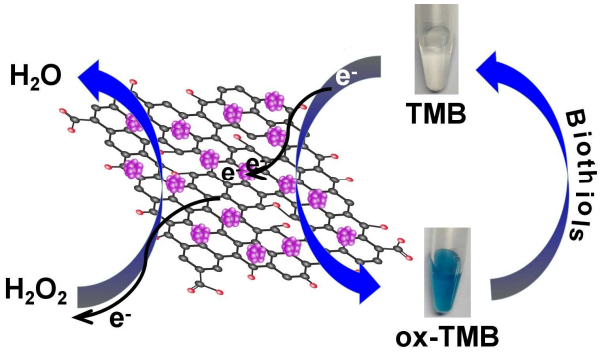

The IrO_2/rGO nanocomposites were prepared by hydrothermal method and showed high peroxidase-like activity, which could catalyze the oxidation of TMB to exhibit deep blue color in the presence of H_2O_2. In the catalytic oxidation process, the TMB molecules were firstly absorbed on the surface of reduced graphene oxide and donated lone-pair electrons to IrO_2 nanoparticles supported on the surface of reduced graphene oxide, leading to an increased electron density of IrO_2 nanoparticles. Then the electron-rich IrO_2 nanoparticles transferred electrons to H_2O_2. Finally, TMB was oxidized into ox-TMB and turned into blue color, and the H_2O_2 was reduced to water. The colorimetric detection of biothiols was established on the basis of the inhibition peroxidase-like activity of IrO_2/rGO.

Facile synthesis of IrO_2/rGO nanocomposites with high peroxidase-like activity for sensitive colorimetric detection of low weight biothiols

Xueliang Liu[a], Xinhuan Wang[a], Qiusen Han[a, b], Cui Qi[a], Chen Wang[a, b], Rong Yang*[a, b]

a. CAS Key Lab for Biomedical Effects of Nanomaterials and Nanosafety, Center of Materials Science and Optoelectronics Engineering, CAS center for Excellence in Nanoscience, National Center for Nanoscience and Technology, University of Chinese Academy of Sciences, Beijing, 100190, P. R. China

b. Sino-Danish College, University of Chinese Academy of Sciences, Sino-Danish Center for Education and Research, Beijing, 100190, P. R. China

*Corresponding author: yangr@nanoctr.cn

Supporting information for this article is available

Abstract

In this work, we reported a novel nanozyme synthesized by decorating highly dispersed ultrafine IrO_2 nanoparticles on reduced graphene oxide (rGO) nanosheets via a simple hydrothermal method. The as-prepared IrO_2/rGO nanocomposites exhibited intrinsic peroxidase-like activity and could catalyze the oxidation of 3,3',5,5'-tetramethylbenzidine (TMB) to produce blue product in the presence of H_2O_2. Catalytic kinetic of IrO_2/rGO nanocomposites followed Michaelis-Menten behavior, exhibiting a higher affinity to TMB than horseradish peroxidase (HRP) enzyme. Catalytic mechanism studies suggested that the peroxidase-like activity of IrO_2/rGO nanocomposites originated from their ability of electron transfer between substrate and H_2O_2. On the basis of high peroxidase-like activity of IrO_2/rGO nanocomposites, a colorimetric strategy for rapid and sensitive detection of low weight biothiols was

developed. The colorimetric detection assays for low weight biothiols showed high selectivity against other amino acids. Therefore, the IrO_2/rGO nanozyme is expected for promising potential applications in the biosensor, diagnostics and environment.

Keywords: IrO_2/rGO nanocomposites; nanozyme; peroxidase-like activity; colorimetric detection; low weight biothiols

1. Introduction

Due to the high specificity and efficiency, protein enzymes are significantly important in the applications of medicine, chemistry and environment[1, 2]. However, the intrinsic drawbacks of natural enzymes including high cost, low stability as well as difficult preparation and purification hinder their practical applications in industry[3]. Therefore, artificial enzyme mimics as alternatives to natural enzymes have been developed during the past few decades. Among them, nanozymes have attracted considerable attention due to the large surface-to-volume ratio and high catalytic activity[4, 5]. Since the first report that the iron magnetic nanoparticles have the intrinsic peroxidase-like activity[6], substantial progress has been achieved. A variety of nanomaterials with peroxidase-like activity have already emerged, such as noble metal nanoparticles[7], metal oxides[8], carbon nanomaterials[9, 10] and metal organic frameworks[11,12], which were applied in biosensor and environment. For instance, the colorimetric detection of bio-molecules, metal ions and bacteria based on their peroxidase-like activity have been developed[13], which benefits the advantages of rapidity, simplicity, low cost and a visual readout.

IrO_2 is one of the best electrocatalysts for the oxygen evolution reaction and has

been widely used in electrocatalytic application[14]. To achieve high catalytic activity and utilization efficiency, considerable efforts have been devoted to synthesize the IrO_2 nanomaterials with controllable nanostructure[15, 16]. However, the IrO_2 nanoparticles are unstable and prone to aggregation, which significantly decreases their catalytic activity. To improve the stability, surfactants are usually introduced, which could occupy the active sites of catalyst and hinder the catalytic activity. The nanoparticles supported on substrates with large surface area was emerged as an alternative method to increase the stability of nanomaterials. Oakton et al[17] reported that IrO_2 nanoparticles with diameter of 1~2 nm dispersed in TiO_2 showed 1.6 times higher mass current density than the pure IrO_2 nanoparticles for the oxygen evolution reaction. The nanocomposites usually exhibit enhanced catalytic activity due to the improved dispersity of catalyst, high surface area of substrate and the synergic effect between catalyst and substrate. However, the enzymatic property of IrO_2 has been barely explored to our knowledge. Graphene oxide (GO) is an ideal substrate for nanocatalysts anchoring in water environment owing to its high surface area and remarkable hydrophilicity[18]. It was also reported that the GO or rGO possessed intrinsic peroxidase-like activity[19, 20]. Meanwhile, the high biocompatibility and low toxicity make GO or rGO as promising candidates for drug delivery and biosensor. Hence, the rational design of IrO_2/rGO nanocomposites could provide a promising strategy to enhance the catalytic property of IrO_2, and develop a new candidate of peroxidase-like nanozyme.

Low weight biothiols play essential roles in the process of metabolism, including

cysteine (Cys), homocysteine (Hcy) and glutathione (GSH) [21]. The concentrations of Cys, Hcy and GSH in serum or plasma of healthy human bodies are approximately in the range of 200~300, 5~15, and 1~5 μM, respectively[22]. The abnormal levels of low weight biothiols are closely relevant to many diseases such as cardiovascular disease, Alzheimer's disease, acquired immunodeficiency syndrome (AIDS) and cancer[23-25]. Therefore, the detection of low weight biothiols is considerable significant for clinical diagnosis and pathology. Despite good selectivity and low detection limit for low weight biothiols, conventional analytical techniques including high-performance liquid chromatography[26], fluorescence[27], electrochemistry[28] and mass spectrometry[29] usually suffer from some inherent issues such as expensive and bulky equipment and time-consuming. Hence, a sensitive and selective biosensor is appealing for the detection of low weight biothiols.

In this work, we reported a facile way to prepare IrO_2/rGO nanocomposites through hydrothermal method. The ultrafine IrO_2 nanoparticles were highly dispersed on the surface of rGO nanosheets. Herein, we demonstrated that IrO_2/rGO nanocomposites displayed enhanced intrinsic peroxidase-like activity owing to the effective catalyzing the oxidation reaction of peroxidase substrates such as 3,3',5,5'-tetramethylbenzidine (TMB), o-phenylenediamine (OPD) and 2,2'-azinobis(3-ethylbenzo-thiazolline-6-sulfonic acid) diammonium salt (ABTS) in the presence of H_2O_2. A sensitive and selective colorimetric method for detection of low weight biothiols was also established based on the inhibition of peroxidase-like activity of IrO_2/rGO nanocomposites.

2. Experimental

2.1 Reagents and materials

Iridium (□) chloride hydrate was purchased from Alfa Aesar (Shanghai, China). Graphite powder, ethanol, hydrogen peroxide solution (30%), dimethylsulfoxide (DMSO), acetic acid and sodium acetate trihydate were obtained from Aladdin Industrial Corporation (Shanghai, China). 3,3',5,5'-tetramethylbenzidine (TMB), o-phenylenediamine (OPD) and 2,2'-azinobis(3-ethylbenzo-thiazolline-6-sulfonic acid) diammonium salt (ABTS) were bought from J&K Scientific Ltd (Beijing, China). Terephthalic acid (TA) was bought from Sinopharm Chemical Reagent Co., Ltd (Shanghai, China). Reduced cytochrome C (Cyt C) was supplied by Abcam (Shanghai, China). Cysteine (Cys), homocysteine (Hcy), glutathione (GSH), arginine (Arg), tryptophan (Trp), tyrosine (Tyr), alanine (Ala), proline (Pro), threonine (Thr), asparagine (Asn), isoleucine (Ile), glutamic (Glu), glutamine (Gln), valine (Val), leucine (Leu), aspartic (Asp), glycine (Gly), serine (Ser), lysine (Lys), methionine (Met), histidine (His) and phenylalanine (Phe) were purchased from Sigma-Aldrich (Shanghai, China). Bovine serum albumin (BSA) was supplied by Beijing Jingke Hongda Biotechnology Co., Ltd. All the chemicals were used as received without any further purification. And the ultrapure water with a resistivity of 18.25 MΩ·cm was supplied by a Millipore Ultrapure water system.

2.2 Preparation of IrO_2/rGO nanocomposites

The GO nanosheets were synthesized from graphite powder by a modified Hummers method[30]. IrO_2/rGO nanocomposites were fabricated by a hydrothermal

method. Typically, 20 mL GO dispersion (1 mg/mL) was mixed with 10 mL $IrCl_3$ solution (1 mg/mL) under vigorous stir. Then the mixture was ultrasonicated for 30 min and transferred into a 50 mL Teflon-lined stainless-steel autoclave. The mixed solution in sealed autoclave was heated to 180□ and held for 10 h. After being cooled to room temperature naturally, the obtained IrO_2/rGO nanocomposites were separated by centrifugation and washed with ultrapure water for three times. The IrO_2 nanoparticles without support was prepared by the same process without GO. And the rGO was also prepared by the same process without $IrCl_3$.

2.3 Peroxidase-like activity of IrO_2/rGO nanocomposites

To investigate the peroxidase-like activity of IrO_2/rGO nnaocomposites, the catalytic oxidation of TMB was carried out in the presence of H_2O_2 at room temperature. The experiments were performed in 1.5 ml tubes. In a typical experiment, 10 μL of TMB (20 mM in DMSO), 10 μL of H_2O_2 (250 mM) and 15 μL of IrO_2/rGO dispersion (IrO_2 concentration 30 μg/mL identified by ICP-OES) were added into acetate buffer solution (0.1 M, pH = 4.0) with a final volume of 500 μL. After 10 min reaction, the absorbance intensity of reaction solution at 652 nm was monitored by an EnVision Multimode Plate Reader. The effects of pH (2.0~7.0), temperature (0~70 °C), H_2O_2 concentration (0~50 mM) and IrO_2/rGO dosage (0~1.5 μg/mL) were evaluated to optimize the catalytic reaction conditions. The steady-state kinetic experiments with TMB were performed by fixing the amount of IrO_2/rGO (0.45 μg: the concentration or amount of catalyst in this work was all calculated by IrO_2 amount.) and concentration of H_2O_2 (5 mM) with various TMB concentrations.

Typically, 465 μL of acetate buffer solution, 10 μL of H_2O_2 (250 mM), 15 μL of IrO_2/rGO dispersion and 10 μL of TMB (different concentrations in DMSO) were added and mixed in 1.5 mL tubes. Then, 200 μL of the mixed solution was added into a 96 well plate and the absorbance intensities at 652 nm were recorded at different time intervals by a Multimode Plate Reader (EnVision). The initial reaction velocity was calculated from the equation: $v = k/h\varepsilon$; where v is the initial velocity, k is the slope of the linear relationship between absorbance intensity and time at first few minutes, ε is the molar absorptivity of ox-TMB (39000 $M^{-1} \cdot cm^{-1}$), and h is the height of solution. Similar kinetic experiments with H_2O_2 were carried out by varying the concentration of H_2O_2 with constant concentration of TMB (0.5 mM) and catalyst (0.45 μg). The Michaelis-Menten parameters were calculated from the linear fitting equation of Lineweaver-Burk plots[31]: $1/v = K_m/v_m$ $(1/[S] + 1/K_m)$; where v is the initial velocity, v_m is the maximal reaction velocity, K_m represents the Michaelis-Menten constant, and [S] is the concentration of substrate.

2.4 The investigation of catalytic reaction mechanism

2.4.1 The effect of iridium ions leaching

Gumpelmayer et al[32] questioned the intrinsic peroxidase-like activity of Fe_3O_4 and claimed that the peroxidase activity of Fe_3O_4 originated from iron ions (Fe^{2+} and Fe^{3+}) leaching. To check the effect of iridium ions releasing, the IrO_2/rGO (2 μg) was firstly added into 2 mL acetate buffer (0.1 M, pH = 4.0) and the solution was incubated for 1 h. After centrifugation at 10000 rpm for 20 min, 500 μL of the supernatant, 10 μL TMB and 10 μL H_2O_2 were added into a 1.5 mL tube and the

absorption spectrum was recorded by an EnVision Multimode Plate Reader from 500 nm ~ 800 nm after 15 min reaction.

2.4.2 Hydroxyl radicals test

As a fluorescence probe, TA is usually used to verify the generation of hydroxyl radicals for the catalytic oxidation reaction in the presence of H_2O_2[33]. TA could capture hydroxyl radicals and produce high fluorescent 2-hydroxy terephthalic acid with the emission peak at 435 nm. Experimentally, 500 μL of acetate buffer (0.1 M, pH = 4) contained 5 mM H_2O_2, 0.5 mM TA and 1.2 μg IrO_2/rGO catalyst was incubated for 30 min at room temperature. Then, the fluorescence spectrum of the solution at 350 nm ~ 600 nm was recorded by a fluorescence spectrophotometer with an excitation wavelength of 315 nm. The fluorescence spectra of solutions without IrO_2/rGO or H_2O_2 were also measured at the same experimental conditions.

2.4.3 Electron transfer experiment

Cyt C was chosen to check the electron transfer role of IrO_2/rGO nanocomposites because the Cyt C is an active reactant in the electron transfer process[34]. In our experiment, 50 μL reduced Cyt C and 1.2 μg IrO_2/rGO catalyst was mixed in 440 μL acetate buffer (0.1 M, pH = 4.0) and incubated at room temperature for 4 h. The absorption spectrum of the solution was recorded by an EnVision Multimode Plate Reader. To exclude the effect of dissolved oxygen, the experiment was repeated under N_2 atmosphere. The control experiment was evaluated at the same experimental conditions without IrO_2/rGO nanocomposites.

2.5 Colorimetric detection of low weight biothiols

Experimentally, 10 μL TMB (20 mM in DMSO), 10 μL H_2O_2 (250 mM), 0.45 μg IrO_2/rGO catalyst and various concentration of biothiols (0~100 μM) were mixed in acetate buffer with final volume of 500 μL. The mixture was incubated at room temperature for 10 min and the absorbance intensity was monitored by the EnVision Multimode Plate Reader. The selective experiments was performed by comparing the color and absorbance intensity of the reaction solutions (10 μL TMB (20 mM in DMSO), 10 μL H_2O_2 (250 mM), 0.45 μg IrO_2/rGO and 460 μL acetate buffer) with different kinds of amino acids at the concentration of 100 μM. To evaluate the practical application, the colorimetric detection of Cys in 5 wt% BSA and human serum solutions with concentration of Cys of 1 mM and 5 mM were carried out. The detection procedure was the same as the colorimetric assay in water.

2.6 Characterization

Transmission electron microscopy (TEM), high-resolution TEM (HRTEM), Energy Dispersive X-ray spectroscopy (EDS), high-angle annular dark-field scanning TEM (HAADF-STEM) and elemental mapping analysis were carried out on a transmission electron microscope (FEI Tecnai G^2 F20, USA) operated at 200 kV to characterize the morphology and component of the prepared IrO_2/rGO nanocomposites. The X-ray powder diffraction (XRD) was collected on a Bruker D8 focus Powder X-ray Diffractometer with Cu Kα radiation at 2θ degree of 5~60°. The Raman spectra were collected by a Renishaw inVia plus Raman Spectrometer with excitation wavelength of 514 nm and acquisition time of 30 s for one measurement. X-ray photoelectron spectroscopy (XPS) was performed on a Thermo Fisher

ESCALAB 250Xi X-ray photoelectron spectrometer. The zeta potentials of nanomaterials were measured on a Malvern Zeta Potential Analyzer (Zetasizer Nano ZS). The composition and concentration of IrO_2/rGO dispersion were measured by an inductive coupled plasma optical emission spectroscopy (ICP-OES, Thermo Scientific, USA). The absorbance and absorption spectra of solutions were recorded on an EnVision Multimode Plate Reader (PerkinElmer, USA) at room temperature. The fluorescence measurements were evaluated by an F-4600 spectrofluorimeter (Hitachi, Japan) with an excitation wavelength of 315 nm and the excitation silt width and emission slit width 5 nm.

3. Results and discussion

3.1 Characterization of IrO_2/rGO nanocomposites

The TEM images (Fig. 1a) clearly demonstrated that the IrO_2 nanoparticles with average size of 1.65 nm were uniformly supported on the surface of rGO, demonstrating the successful preparation of IrO_2/rGO nanocomposites. The TEM images of GO and rGO were displayed in Fig. S1. GO showed a sheet-like morphology, which transformed to creased structure after hydrothermal reaction, indicating the formation of rGO. The color of GO also changed from light yellow to black (Fig. S2). The average size of IrO_2 nanoparticles on the surface of rGO nanosheets was estimated to be 1.65 nm according to the particle size distribution by counting more than 200 nanoparticles (Fig. S3). As an efficient carrier, the rGO could effectively prevent the aggregation of IrO_2 nanoparticles. The HRTEM (inset Fig. 1a) clearly showed the d-spacing value of 0.26 nm, which was consistent with the (101)

plane of IrO_2 (JPDS No. 15-0870)[35]. The HAADF-STEM image and EDS elemental mapping analysis were employed for further investigating the morphology and composition of IrO_2/rGO nanocomposites. The HAADF image (Fig.1c) clearly showed the ultrafine IrO_2 nanoparticles uniformly dispersed on the surface of rGO nanosheets. The EDS elemental mapping analysis (Fig. S4 and Fig. 1d-g) showed the homogeneous C, O and Ir species, confirming the ultrafine IrO_2 nanoparticles uniformly dispersed on the support.

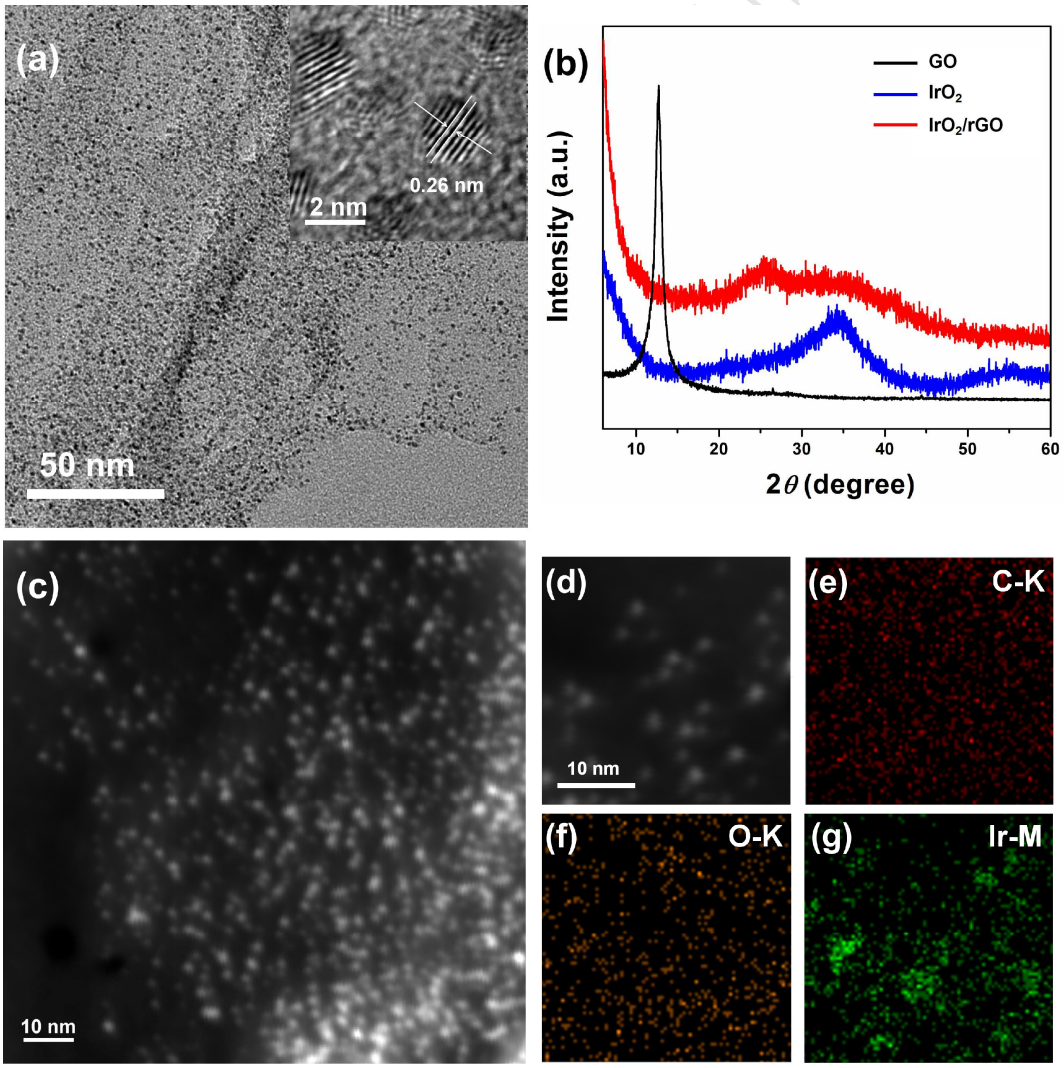

Fig.1 (a) TEM images of IrO_2/rGO nanocomposites, inset the HRTEM image, (b) the

XRD patterns of GO, IrO_2 and IrO_2/rGO, (c) the HAADF image of IrO_2/rGO and (d)-(f) the EDS elemental mapping images of IrO_2/rGO with C, O and Ir species.

The XRD patterns of GO nanosheets, IrO_2 nanoparticles and IrO_2/rGO nanocomposites were presented in Fig. 1b. A broad and weak diffraction peak of IrO_2 nanoparticles (Fig. 1b blue line) at 34.5° corresponded to the (101) plane of IrO_2, which was consistent with the HRTEM analysis. A sharp diffraction peak of GO nanosheets was observed at 2θ degree of 12.5°, corresponding to the (001) plane[36]. However, no diffraction peak at 12.5° was observed in IrO_2/rGO nanocomposites patterns, illustrating the reduction of GO at high temperature. According to the Raman spectra (Fig. S5), the ratio of D peak and G peak of GO and IrO_2/rGO was 0.83 and 0.95, respectively. The increase of D/G ratio also suggested the reduction of GO by hydrothermal reaction[37]. A new broad diffraction peak at 2θ of 25.4° appeared, which implied the poor order stacking of rGO nanosheets. There were no apparent IrO_2 diffraction peaks due to the small particle size of IrO_2.

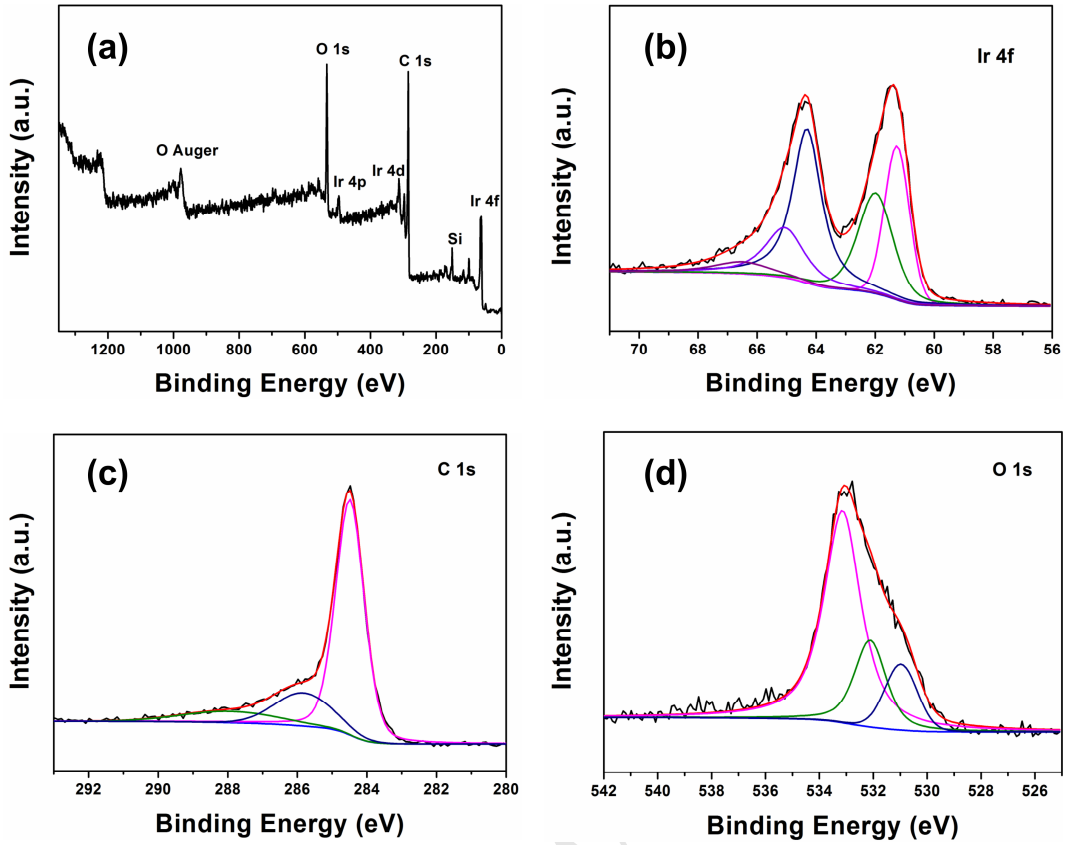

Fig. 2 The XPS spectra of IrO_2/rGO nanocomposites. (a) Survey spectrum, (b) the high resolution spectra of Ir 4f, (c) the high resolution spectra of C 1s and (d) the high resolution spectra of O 1s.

X-ray photoelectron spectroscopy was employed to investigate the chemical states of IrO_2/rGO nanocomposites. The survey spectrum with strong peak intensity of C, O and Ir species was given in Fig. 2a. The high resolution XPS spectra of Ir 4f, C 1s and O 1s were further investigated. As shown in Fig. 2b, the peaks at 64.4 and 61.3 eV could correspond to the binding energies of Ir $4f_{5/2}$ and Ir $4f_{7/2}$ of IrO_2. The peaks at 65.0 and 66.6 eV could attribute to the satellite peaks of Ir $4f_{5/2}$ (IrO_2) and the peak at 62.0 eV could be ascribed to the satellite peak of Ir $4f_{7/2}$ (IrO_2). The 4f binding energy of IrO_2 nanoparticles shifted 0.4 eV towards higher binding energy compared to the IrO_2/rGO nanocomposites (Fig. S6a), which could be attributed to the Ir^{3+} ions

in IrO_2 nanoparticles[38]. And the high resolution XPS spectra of Ir 4f of IrO_2 nanoparticles were presented at Fig. S6b. Fig. 2c presented the high resolution C 1s spectra of IrO_2/rGO. The main peak at 284.5 eV was assigned to the C-C bond, and the peaks at binding energies of 285.8 and 288.4 eV were attributed to the C-O and O-C=O bonds of rGO[39]. The peaks at 533.3 eV and 532.2 eV were ascribed to O-C=O and C-O functional groups on rGO (Fig. 2d), and the peak located at 531.0 eV was indexed to the -OH groups on rGO and IrO_2. The content of oxygen element in C-O and -OH significantly decreased compared to the O 1s spectra of GO (Fig. S7b), which also proved the reduction of GO after hydrothermal reaction, which was in consistence with the results of XRD patterns and Raman analysis.

3.2 Peroxidase-like activity of IrO_2/rGO nanocomposites

The peroxidase-like activity of IrO_2/rGO nanocomposites was evaluated by catalytic oxidation of several chromogenic substrates (such as TMB, OPD and ABTS) in the presence of H_2O_2. The solution color of TMB, OPD and ABTS changed from colorless to blue, orange and green respectively (Fig. 3a), which indicated the peroxidase-like activity of IrO_2/rGO nanocomposites. The enzymatic activity of rGO, IrO_2 nanoparticles, IrO_2 and rGO mixture were further evaluated and compared with IrO_2/rGO nanocomposites (Fig. 3b). After adding the IrO_2/rGO, the reaction solution changed from colorless to deep blue color and exhibited a maximum absorbance at 652 nm, revealing the high peroxidase-like activity of IrO_2/rGO nanocomposites (Fig. 3b-6). In contrast, the TMB and H_2O_2 reaction solution in the absence of catalysts showed negligible color change (Fig. 3b-2), suggesting that the IrO_2/rGO

nanocomposites were responsible for the catalytic oxidation of TMB. The rGO nanosheets and IrO_2 nanoparticles also showed peroxidase-like activity to some extent (Fig. 3b-3 and b-4). The absorbance of TMB solution at 652 nm with IrO_2/rGO catalyst was the highest. Obviously, the catalytic activity of IrO_2/rGO nanocomposites was much higher than IrO_2 and rGO mixture, IrO_2 nanoparticles or rGO nanosheets. The enhanced catalytic activity of IrO_2/rGO nanocomposites mainly originated from the monodisperse IrO_2 nanoparticles on the surface of rGO nanosheets, while the aggregation of IrO_2 nanoparticles without support severely decreased the catalytic activity of IrO_2 nanoparticles. The IrO_2/rGO nanocomposites could not catalyze the oxidation of TMB in the absence of H_2O_2 (Fig. S8). All these results confirmed that the IrO_2/rGO nanocomposites exhibited the intrinsic peroxidase-like activity.

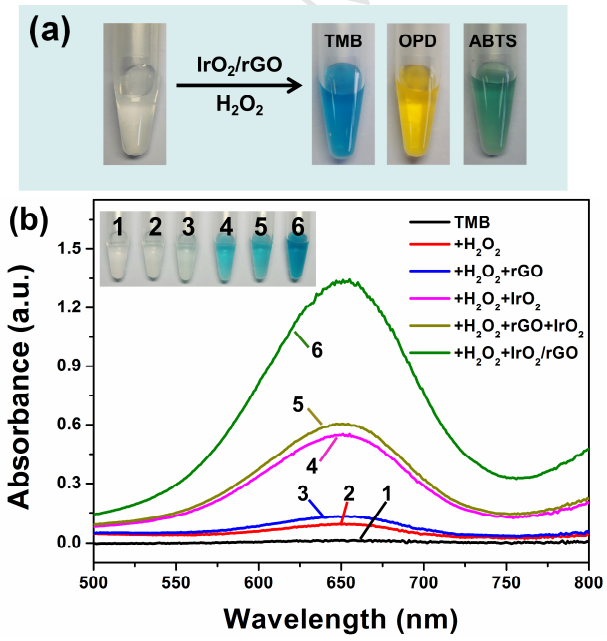

Fig. 3 (a) The photographs of TMB, OPD and ABTS solution after catalytic oxidation by IrO_2/rGO nanocomposites in the presence of H_2O_2, and (b) UV-vis absorption spectra of (1): TMB, (2): TMB+H_2O_2, (3): TMB+rGO+H_2O_2, (4): TMB+IrO_2+H_2O_2,

(5): TMB+H_2O_2+IrO_2 and rGO mixture and (6): TMB+IrO_2/rGO+H_2O_2 solution after mixing for 15 min (inset: the color change of the corresponding solutions).

Similar to natural peroxidase and other nanozymes, the peroxidase-like activity of IrO_2/rGO nanocomposites strongly depended on the reaction conditions including pH, temperature, reaction time and the concentrations of H_2O_2, TMB and catalyst. The optimal pH value was approximately 4.0, which was confirmed by varying the buffer pH value from 2.0 to 7.0 (Fig. S9a). The peroxidase-like activity of IrO_2/rGO nanocomposites increased with temperature and reached the highest activity at 55 °C (Fig. S9b). The decrease activity of IrO_2/rGO over 55°C might be assigned to the decomposition of oxidized TMB (ox-TMB)[40] and the color of solution was from blue to green at 55°C. To simplify the experiment, we carried out all the colorimetric reaction at room temperature. The catalytic activity increased with the concentration of H_2O_2 and no inhibition effect was observed at high concentration of H_2O_2 (Fig. S9c). Furthermore, the absorbance of reaction solution increased with the increase amount of IrO_2/rGO catalyst and presented a linear relationship between the absorbance of oxidized TMB and the concentration of IrO_2/rGO catalyst (Fig. S9d). The experiment parameters with pH value of 4.0 and concentrations of TMB 0.4 mM, H_2O_2 5 mM, and IrO_2/rGO 0.9 μg/mL were chosen in the following colorimetric detection assay at room temperature.

The peroxidase-like performance of the IrO_2/rGO nanocomposites was further explored by the steady-state kinetics. The kinetic data were acquired by varying the

H_2O_2 concentrations at a constant TMB concentration and vice versa. The results were presented in Fig. 4. And the time-dependent absorbance changes at 652 nm were displayed in Fig. S10. The steady-state kinetics experiments of IrO_2/rGO nanocomposites to OPD and ABTS were also carried out at the same procedure and the results were shown in Fig. S11 and Fig. S12. The relationship between the initial reaction rate and the concentration of substrate fitted well with the Michaelis-Menten equation. The Michaelis-Menten constant K_m and the maximal reaction velocity v_{max} were calculated by the linear fitting equation of Lineweaver-Burk plot and listed in Table S1. It is believed that a smaller K_m represents a higher affinity to the substrate[41]. The K_m value of IrO_2/rGO nanocomposites with TMB as the substrate (0.276 mM) was lower than that of HRP (0.434 mM)[6], suggesting an apparently higher affinity to TMB than HRP. The highest K_m value of IrO_2/rGO nanocomposites with ABTS (Table S1) implied the lowest affinity to ABTS compared to TMB and OPD, which could be attributed to the repulsion of the ABTS anions and negative surface charge of IrO_2/rGO nanocomposites (Fig. S13). The K_m value of the IrO_2/rGO nanocomposites for H_2O_2 was 60 times higher than that of HRP (Table S1), indicating a lower affinity but higher endurance to H_2O_2. The above results declared that the IrO_2/rGO nanocomposites possessed high peroxidase-like activity and were good potential candidates for enzymatic mimic.

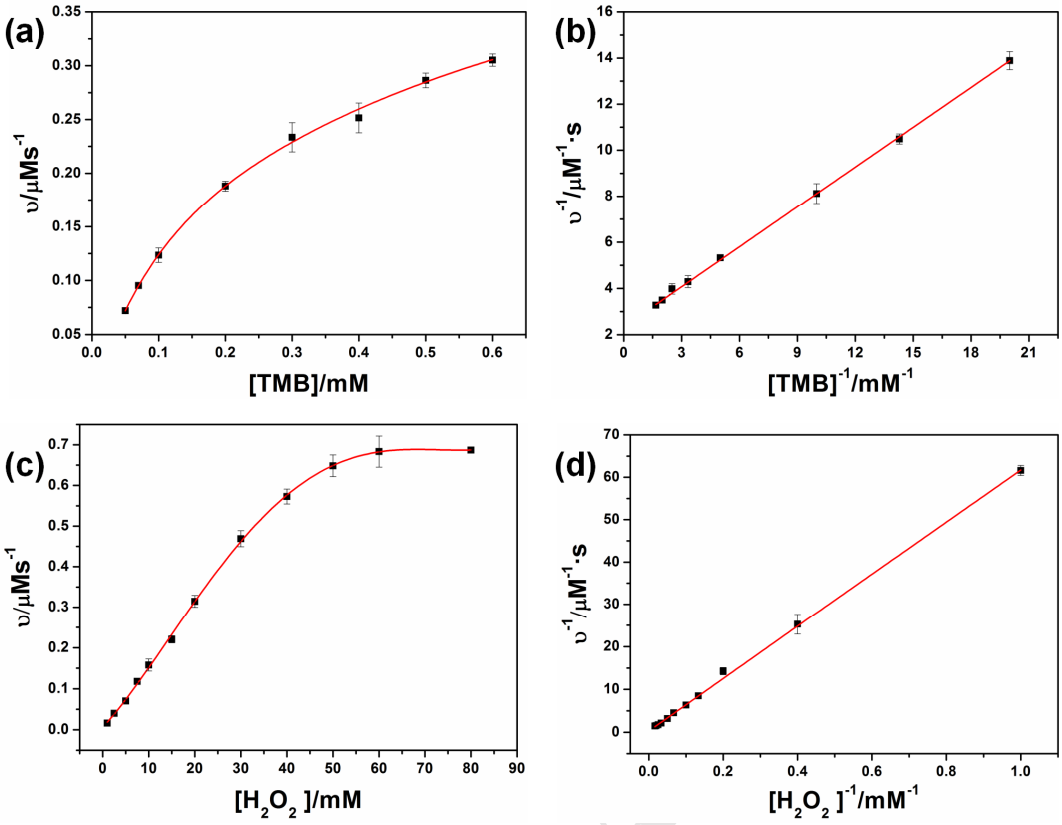

Fig. 4 Steady-state kinetic assay of IrO_2/rGO nanocomposites: TMB concentration (a) and H_2O_2 concentration (c) dependence of initial reaction velocity (*v*); Double reciprocal plots between reaction velocity and TMB concentration (b) and H_2O_2 concentration (d).

3.3 The mechanism of peroxidase-like activity of IrO_2/rGO nanocomposites

Fig. 5a showed the results of iridium ions leaching experiment. The absorbance intensity of ox-TMB solution with the iridium ions leaching for 1 h were comparable to the control experiment, which were negligible compared to intensity of the solution with IrO_2/rGO nanocomposites. We presumed that the iridium ions had no effect on the oxidation of TMB or there were no iridium ions released in 0.1 M acetate buffer with pH value of 4.0. The experimental results demonstrated that the peroxidase-like

activity of IrO_2/rGO nanocomposites did not originate from the iridium ions leaching.

Besides metal ions releasing, the generation of hydroxyl radical and the electron transfer process are the two main pathways of catalytic oxidation. To clarify the catalytic mechanism of IrO_2/rGO nanocomposites, terephthalic acid (TA), a fluorescence probe for hydroxyl radical, was firstly used to check the generation of hydroxyl radical. As shown in Fig. 5b, there was no fluorescence of TA at 435 nm without H_2O_2 (red line). A strong fluorescence peak at 435 nm was observed in TA and H_2O_2 reaction system, revealing the generation of hydroxyl radical by the intrinsic decomposition of H_2O_2. The fluorescence intensity decreased when rGO was added, which proved that rGO could quench the hydroxyl radical. When the IrO_2/rGO nanocomposites were added into the TA and H_2O_2 reaction solution, the fluorescence intensity decreased significantly. The results declared that the IrO_2/rGO catalyst could scavenge hydroxyl radicals rather than promoting the generation of them, which excluded the effect of hydroxyl radical on peroxidase-like activity of IrO_2/rGO nanocomposites.

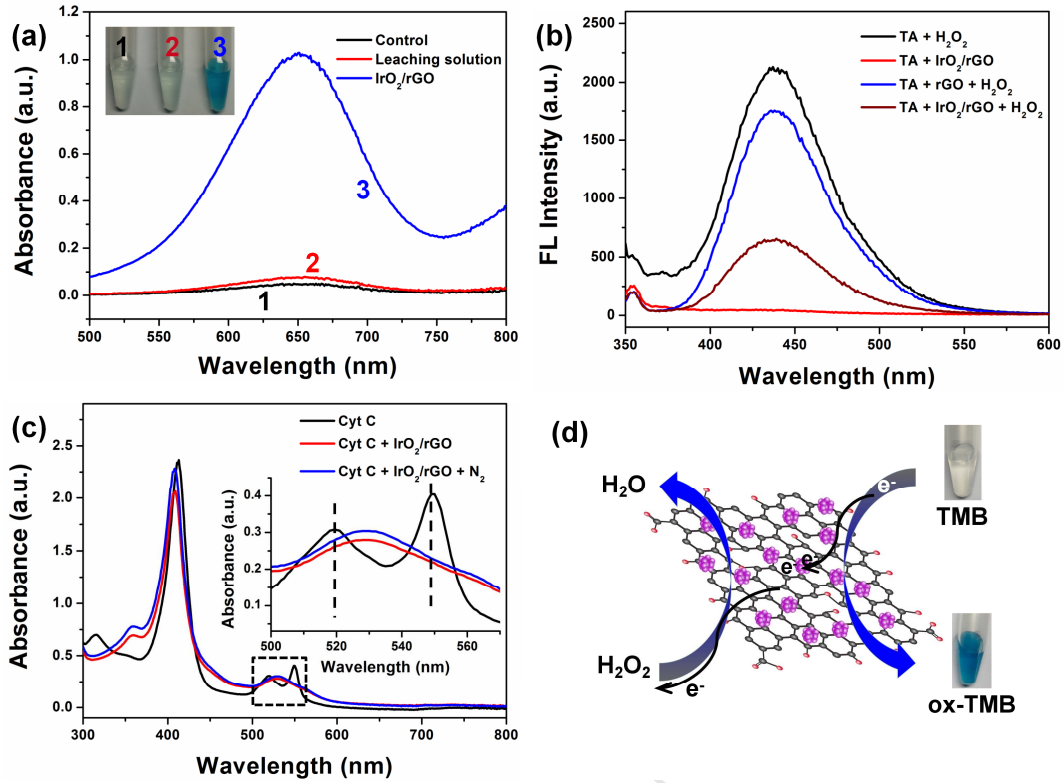

Fig. 5 The mechanism studies of peroxidase-like activity of IrO_2/rGO. (a) Iridium ion leaching experiment: (1) TMB+H_2O_2, (2) TMB+H_2O_2 with iridium ions solution and (3) TMB+IrO_2/rGO+H_2O_2, (b) fluorescence emission spectra of TA in different reaction solutions, (c) UV-vis absorption spectra of reduced Cyt C, Cyt C with IrO_2/rGO and Cyt C with IrO_2/rGO under N_2 atmosphere and (d) schematic illustration of the mechanism of the peroxidase-like activity of IrO_2/rGO nanocomposites.

Cytochrome C (Cyt C) was chosen to verify the mediator role of the IrO_2/rGO catalyst in the electron transfer process from TMB to H_2O_2. As shown in Fig. 5c, there were two intrinsic absorption peaks of reduced Cyt C at 520 nm and 550 nm. After incubation with IrO_2/rGO for 4 h, the original two peaks disappeared with the evolution of a new absorption peak at 530 nm, suggesting that the Cyt C changed

from reduced state to oxidized state. The same results were obtained at nitrogen atmosphere, which excluded the effects of dissolved oxygen. The results clearly demonstrated the electron transfer from Cyt C to IrO_2/rGO nanocomposites. Besides, the electron transfer abilities of IrO_2 nanoparticles and rGO were also performed at the same experimental procedure. The reduced Cyt C was changed to oxidation state after incubation with IrO_2 nanoparticles, while rGO had little effect on the oxidation/reduction state of Cyt C (Fig. S14). The peroxidase-like activity of IrO_2/rGO nanocomposites could mainly originate from the electron transfer abilities of IrO_2 nanoparticles on the surface of rGO.

Based on the experimental results, we deduced that the IrO_2/rGO nanocomposites performed as electron transfer mediators between TMB and H_2O_2 and the mechanism could be illustrated by Fig. 5d. Firstly, the TMB molecule was adsorbed on the surface of rGO and donated lone-pair electrons to IrO_2 nanoparticles supported on the surface of rGO, leading to an increased electron density of IrO_2 nanoparticles. Then the electron-rich IrO_2 nanoparticles transferred electrons to H_2O_2, which accelerated the electron transfer from IrO_2/rGO nanocomposites and TMB substrate. Finally, TMB was oxidized into ox-TMB and turned into blue color, and the H_2O_2 was reduced to water.

3.4 Colorimetric detection of biothiols

The color changes of TMB+H_2O_2+IrO_2/rGO reaction solution were explored for the determination of biothiols based on the relationship between the absorbance intensity and the concentrations of biothiols. As shown in Fig. 6a, the color of the

reaction solution gradually changed from deep blue to colorless with the increase of Cys concentration. The absorption peak of ox-TMB at 652 nm decreased with the concentration of Cys increasing. The value of absorbance intensity at 652 nm exhibited a good linear relationship to the logarithm of Cys concentration in the range of 0.1~50 μM with a correlation coefficient (R^2) of 0.99425 (Fig. 6b). The calculated detection limit for Cys was 40 nM at an S/N ratio of 3. The colorimetric detection of Hcy and GSH were also carried out under the same experimental conditions. Similar to Cys, the absorbance intensity of reaction solution and the logarithm of concentration of GSH and Hcy displayed good linear correlation in the concentration range of 0.1~50 μM (Fig. S15 and Fig. S16). The theoretical capability of detection for Hcy and GSH was 57 nM and 83 nM, respectively. Based on the value of theoretical capability, the sensitivity value of IrO_2/rGO nanozyme responding to biothiols was Hcy > GSH > Cys.

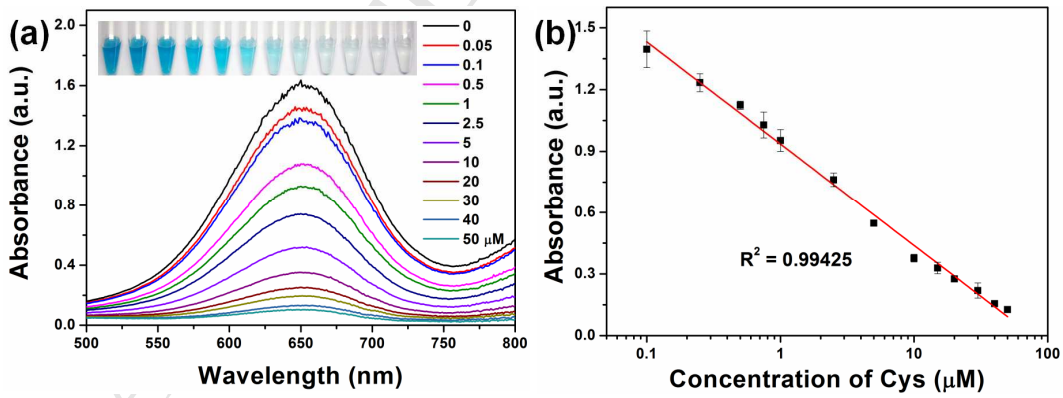

Fig. 6 (a) UV-vis absorption spectra of reaction solutions (TMB 0.4 mM, H_2O_2 5mM and IrO_2/rGO 0.9 μg/mL) in the presence of various concentrations of Cys (inset: the corresponding photographs of reaction solutions). (b) The linear relationship between absorbance intensity and the logarithm of concentration of Cys after 15 min reaction.

In addition, the selectivity of the current approach was investigated by testing nineteen kinds of amino acids besides Cys, Hcy and GSH with the same concentration. Fig. 7 presented the absorbance and color change of the reaction solutions with different amino acids and low weight biothiols. Compared to the control experiment, the color of the solution were almost unchanged after adding the nineteen amino acids. However, the solutions were almost colorless after adding the Cys, Hcy and GSH, and the absorbance intensity declined significantly. The results demonstrated that the developed colorimetric sensor showed high selectivity for low weight biothiols. To explore the practical usability of the proposed colorimetric assay, we detected the concentration of Cys in 5 wt% BSA and human serum, respectively. As shown in Table S2, the experimental results agreed well with the added content in BSA. There was some difference between the detected amount of Cys and added content in serum samples, which could be attributed to the complicated components of serum.

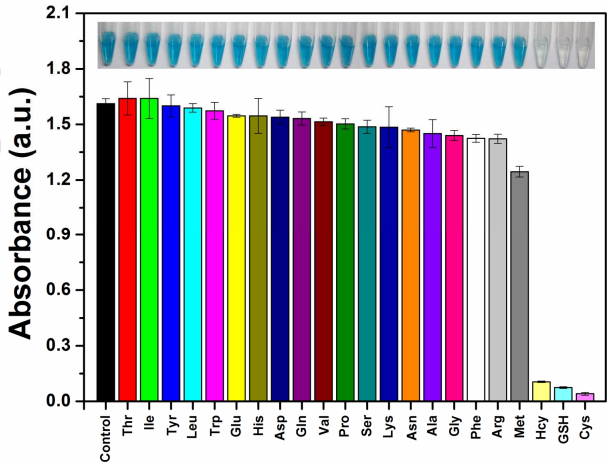

Fig. 7 Selectivity for low weight biothiols to other amino acids with all substances concentration of 50 μM, inset: photographic images of solution after 15 min reaction.

4. Conclusions

The ultrafine IrO_2/rGO nanocomposites with high intrinsic peroxidase mimetic properties were synthesized by a simple hydrothermal method without any surfactant. The peroxidase-like activity of IrO_2/rGO catalyst depended on the pH, temperature and concentration of substrate similar to HRP. The steady-state kinetic study demonstrated that the peroxidase-like activity of IrO_2/rGO nanocomposites followed the Michaelis-Menten theory. Mechanistic research suggested that the ability of IrO_2/rGO nanocomposites acting as electron transfer mediators was responsible for the peroxidase mimetic property rather than the generation of hydroxyl radicals or iridium ions leaching. The colorimetric assays for sensitive and selective detection of low weight biothiols were established based on the induced inhibition of the peroxidase-like activity of IrO_2/rGO nanocomposites. This work provided a novel material with high enzyme mimetic activity and showed promising application in biosensor.

Acknowledgments

This work was supported by National key research and development program from the Ministry of Science and Technology of China (2016YFC0207102) and National Natural Science Foundation of China (21573050).

Reference

1 S. Jemli, D. Ayadi-Zouari, H.B. Hlima and S. Bejar, Biocatalysts: application and engineering for industrial purposes, Crit. Rev. Biotechnol. 36 (2015) 246-258.

2 A.J. Kirby, Enzyme-Mechanismen, Modellreaktionen und Mimetica, Angew. Chem. 108 (2006) 770-790.

3 Y. Yin, Z. Dong, Q. Luo and J. Liu, Biomimetic catalysts designed on macromolecular scaffolds, Prog. Polym. Sci. 37 (2012) 1476-1509.

4 M. Nasir, M.H. Nawaz, U. Latif, M. Yaqub, A. Hayat and A. Rahim, An overview on enzyme-mimicking nanomaterials for use in electrochemical and optical assays, Microchim. Acta. 184 (2016) 1-20.

5 E. Kuah, S. Toh, J. Lee, Q. Ma and Z. Gao, Enzyme mimics: advances and applications, Chem. Eur. J. 25 (2016) 8404-8430.

6 L. Gao, J. Zhuang, L. Zhang, Y. Zhang, N. Gu, T. Wang, J. Feng, D. Yang and S. Perrett, Intrinsic peroxidase-like activity of ferromagnetic nanoparticles, Nat. Nanotechnol. 2 (2007) 577-583.

7 D. Pedone, M. Moglianetti, L.E. De, G. Bardi and P.P. Pompa, Platinum nanoparticles in nanobiomedicine, Chem. Soc. Rev. 46 (2017) 4951-49755.

8 S. Rajeshkumar and P. Naik, Synthesis and biomedical applications of Cerium oxide nanoparticles-A Review, Biotechnol. Rep. 17 (2018) 1-5.

9 H. Sun, Y. Zhou, J. Ren, X. Xu, Carbon nanozymes: Enzymatic properties, catalytic mechanism, and applications, Angew. Chem. Int. Edit. 57 (2018) 9224-9237.

10 M. Chen, G. Zeng, P. Xu, Y. Zhang,, D. Jiang and S. Zhou, Understanding enzymatic degradation of single-walled carbon nanotubes triggered by functionalization using molecular dynamics simulation, Environ. Sci. Nano. 4 (2017) 720-727.

11 Y. Xiong, S. Chen, F. Ye, L. Su, C. Zhang, S. Shen and S. Zhao, Synthesis of a mixed valence state Ce-MOF as an oxidase mimetic for the colorimetric detection of biothiols, Chem. Commun. 51 (2015) 4635-4638.

12 H. Tan, C. Ma, L. Gao, Q. Li, Y. Song, F. Xu, T. Wang and L. Wang, Metal-organic framework-derived copper nanoparticle@carbon nanocomposites as peroxidase mimics for colorimetric sensing of ascorbic acid, Chem. Eur. J. 20 (2014) 16377-16383.

13 Y. Song, W. Wei and X. Qu, Colorimetric biosensing using smart materials, Adv. Mater. 23 (2011) 4215-4236.

14 Antolini, E., Iridium as catalyst and cocatalyst for oxygen evolution/reduction in acidic polymer electrolyte membrane electrolyzers and fuel cells, ACS Catal. 4 (2014) 1426–1440.

15 G. Li, S. Li, M. Xiao, J. Ge, C. Liu and W. Xing, Nanoporous IrO_2 catalyst with enhanced activity and durability for water oxidation owing to its micro/mesoporous structure, Nanoscale. 9 (2017) 9291-9298.

16 Y. Lee, M. Kang, J.H. Shim, N.S. Lee, J.M. Baik, Y. Lee, C. Lee and M.H. Kim, Growth of highly single crystalline IrO_2 nanowires and their electrochemical applications, J. Phys. Chem. C 116 (2013) 18550–18556.

17 E. Oakton, D. Lebedev, M. Povia, D. F. Abbott, E. Fabbri, A. Fedorov, M. Nachtegaal, C. Coperet and T. J. Schmidt, IrO_2-TiO_2: A high-surface-area, active, and stable electrocatalyst for the oxygen evolution reaction, ACS Catal. 7 (2017) 2346-2352.

18 G. Reina, J.M. González-Domínguez, A. Criado, E. Vázquez, A. Bianco and M. Prato, Promises, facts and challenges for graphene in biomedical applications., Chem. Soc. Rev. 46 (2017) 4400-4416.

19 Y. Song, K. Qu, C. Zhao, J. Ren, X. Qu, Graphene oxide: Intrinsic peroxidase catalytic activity and its application to glucose detection, Adv. Mater. 22 (2010) 2206-2210.

20 Y. Hu, X. Gao, Y. Zhu, F. Muhammad, S. Tan, W. Cao, S. Lin, Z. Jin, X. Fa, H. Wei, Nitrogen-doped carbon nanomaterials as highly active and specific peroxidase mimics, Chem. Mater. 30 (2018) 6431-6439.

21 M. H. Stipanuk, Sulfur amino acid metabolism: pathways for production and removal of homocysteine and cysteine, Annu. Rev. Nutr. 24 (2004) 539-577.

22 I. Muneki, K. Takahiro, F. Takashi and T. Makoto, Analytical methods involving separation techniques for determination of low-molecular-weight biothiols in human plasma and blood, J. Chromatogr. B 964 (2014) 103-115.

23 Y. M. Go, D. P. Jones, Cysteine/cystine redox signaling in cardiovascular disease, Free Radical Bio. Med. 50 (2011) 495-509.

24 S. Seshadri, A. Beiser, J. Selhub, P. F. Jacques, I. H. Rosenberg, R. B. D'Agostino, P. W. F. Wilson, P. A. Wolf, Plasma homocysteine as a risk factor for dementia and Alzheimer's disease, New Engl. J. Med. 346 (2002) 476-483.

25 G. Wu, Y. Fang, S. Yang, J. R. Lupton, N. D. Tuner, Glutathione metabolism and its implications for health. J. Nutr. 134 (2004) 489-492.

26 Y. Zu, Molecular and nanoparticle postcolumn reagents for assay of low-molecular-mass biothiols using high-performance liquid chromatography, J. Chromatogr. B 877 (2009) 3358-3365.

27 C. Yin, K. Xiong, F. Huo, J.C. Salamanca, R.M. Strongin, Fluorescent probes with multiple binding sites for the discrimination of Cys, Hcy and GSH, Angew. Chem. Int. Edit. 56 (2017) 13188-13198.

28 M. Alagiri, P. Rameshkumar, A. Pandikumar, Gold nanorod-based electrochemical sensing of small biomolecules: a review, Microchim. Acta 184 (2017) 3069-3092.

29 N. Burford, M.D. Eelman, D.E. Mahony, M. Morash, Definitive identification of cysteine and glutathione complexes of bismuth by mass spectrometry: assessing the biochemical fate of bismuth pharmaceutical agents, Chem. Commun. 1 (2003) 146-147.

30 J. Chen, B.W. Yao, C. Li and G.Q. Shi, An improved Hummers method for eco-friendly synthesis of graphene oxide, Carbon 64 (2013) 225-229.

31 W. Li, B. Chen, H. Zhang, Y. Sun, J. Wang, J. Zhang and Y. Fu, BSA-stabilized Pt nanozyme for peroxidase mimetics and its application on colorimetric detection of mercury(II) ions, Biosens. Bioelectron. 66 (2015) 251-258.

32 M. Gumpelmayer, M. Nguyen, G. Molnár, A. Bousseksou, B. Meunier and A. Robert, Magnetite Fe_3O_4 has no intrinsic peroxidase activity, and is probably not involved in Alzheimer's oxidative stress, Angew. Chem. Int. Edit. 57 (2018) 14758-14763.

33 J. Mu, Y. Wang, M. Zhao and L. Zhang, Intrinsic peroxidase-like activity and catalase-like activity of Co_3O_4 nanoparticles, Chem. Commun. 48 (2012) 2540-2542.

34 J. Dong, L. Song, J. J. Yin, W. He, Y. Wu, N. Gu and Y. Zhang, Co_3O_4 nanoparticles with multi-enzyme activities and their application in immunohistochemical assay, ACS Appl. Mater.

Inter. 6 (2014) 1959-1970.

35 K. Guo, Y. Li, T. Yuan, X. Dong, X. Li and H. Yang, Ultrafine IrO_2 nanoparticle-decorated carbon as an electrocatalyst for rechargeable Li-O_2 batteries with enhanced charge performance and cyclability, J. Solid State Electr. 19 (2015) 821-829.

36 R. Krishna, E. Titus, L. C. Costa, J.C Menezes, M. Correia, S. Pinto, J. Ventura, J. P. Araújo, J. Cavaleiro and J. Gracio, Facile synthesis of hydrogenated reduced graphene oxide via hydrogen spillover mechanism, J. Mater. Chem. 22 (2012) 10457-10459.

37 S. Pei and H.M. Cheng, The reduction of graphene oxide, Carbon 50 (2012) 3210-3228.

38 V. Pfeifer, T.E. Jones, J.J.V. Vélez, C. Massué, R. Arrigo, D. Teschner, F. Girgsdies, M. Scherzer, M.T. Greiner, J. Allan, M. Hashagen, G. Weinberg, S. Piccinin, M. Hävecker, K.G. Axel, R. Schlögl, The electronic structure of iridium and its oxides, Surf. Interface Anal. 48 (2016) 261-273.

39 W. Gao, The chemistry of graphene oxide, Graphene Oxide (2015) 61-95.

40 M. Cui, J. Zhou, Y. Zhao and Q. Song, Facile synthesis of iridium nanoparticles with superior peroxidase-like activity for colorimetric determination of H_2O_2 and xanthine, Sensor. Actuat. B Chem. 243 (2017) 203-210.

41 Y. Liu and F. Yu, Substrate-specific modifications on magnetic iron oxide nanoparticles as an artificial peroxidase for improving sensitivity in glucose detection, Nanotechnology 22 (2011) 145704-145711.

IrO_2 nanoparticles homogeneously supported on reduced graphene oxide

The IrO_2/rGO nanocomposites exhibited enhanced peroxidase-like activity

The peroxidase-like activity originated from the electron transfer mechanism

Sensitive and selective colorimetric detection of low-molecular-weight biothiols